

Applications of Hydrogen Silsesquioxane in Nanomanufacturing and Nanofabrication

Yuping Xu*, Yunzi Xin*, Takashi Shirai **

*Advanced Ceramics Research Center, Nagoya Institute of Technology,
Gokiso-cho, Showa-ku, Nagoya, Aichi 466-8555, JAPAN

**Department of Life Science and Applied Chemistry,
Graduate School of Engineering, Nagoya Institute of Technology,
Gokiso-cho, Showa-ku, Nagoya, Aichi 466-8555, JAPAN

Abstract: Hydrogen silsesquioxane (HSQ) is a versatile inorganic material that has garnered significant attention in the semiconductor industry, such as in micro-/nano-electromechanical systems, photonic devices, and nanoelectronics, owing to its high silicon content, small molecular size, low dielectric constant, excellent line edge roughness, high etching resistance, and local planarization capabilities. This review article discusses the application-related aspects of HSQ in nanomanufacturing for integrated circuits and nanoscale patterning, and the technical applications of HSQ in the fabrication of semiconductor silicon-based nanomaterials.

Hydrogen silsesquioxane (HSQ), a completely inorganic silsesquioxane first synthesized by Collins and Frye in 1970^[1], has a general chemical composition of $(\text{HSiO}_{1.5})_n$, including commercial $(\text{H}_8\text{Si}_8\text{O}_{12})$ ($n = 8$) cubic clusters and laboratory-synthesized $(\text{HSiO}_{1.5})_n$ ($n > 8$) polymers. HSQ has a cage-like structure (Fig. 1-a) and a random network of partially formed cages (Fig. 1-b). Cage-like silsesquioxanes are typically referred to as polyhedral oligosilsesquioxanes or polyhedral oligomeric silsesquioxanes. This class of well-defined, highly symmetric molecules usually features a nanoscopic size of approximately 1–3 nm in diameter, which can be regarded as one of the smallest possible silica particles. Molecules with a T_8 cubic inorganic core composed of silicon–oxygen ($\text{H}_8\text{Si}_8\text{O}_{12}$) linkages are the most prevalent systems studied. As a critical alternative to commercial cubic clusters, the HSQ polymer $(\text{HSiO}_{1.5})_n$ ($n > 8$) can be easily synthesized by mixing water and trichlorosilane in a short time via hydrolysis and polycondensation reactions in a one-pot reaction with a yield as high as $\sim 95\%$ ^[1–3]. In short, HSQ is commercially available in methyl isobutyl ketones as a flowable oxide (Fox) or is synthesized with a high degree of purity, which makes it ideal for use in nanofabrication and other high-tech applications where purity is important. HSQ exhibits a low dielectric constant, ranging from 2.6 and 3, making it a good insulator for use in electronic devices^[4]. Owing to its high silicon content, HSQ is resistant to oxygen plasma and it exhibits a sufficiently high etching resistance^[5–7].

HSQ is also appreciated for its excellent line-edge roughness and local planarization capabilities^[8]. In the early 1990s, HSQ was used as a carbonless protective coating and interlayer dielectric material in high-performance integrated circuits in the semiconductor industry^[9–13]. In 1998, Namatsu et al. discovered HSQ as an inorganic negative-tone resistance for electron beam lithography (EBL)^[5, 14]. Based on these findings, the semiconductor grade HSQ has already been an industrial standard negative-tone resist applicable for high resolution and small linewidth fluctuations electron-beam patterns^[15–28], extreme ultraviolet (EUV) lithography^[29–36], proton beam writing^[37, 38], molding material in nanoimprint lithography^[39–47], step and flash imprint lithography^[48], and making masks using dry etching processes^[49–53]. In addition to creating physical patterns, HSQ can be engineered to exhibit a wide range of functional properties that transcend the notion of

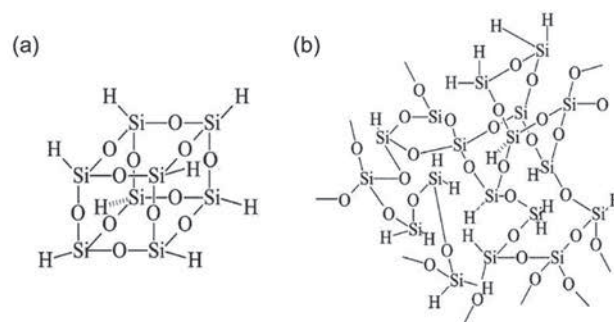


Figure 1. Chemical structures of HSQ: (a) cage form, (b) network form.

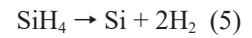
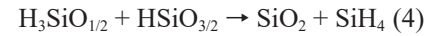
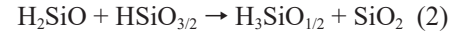
resists being used singularly as sacrificial components to transfer a pattern into functional materials. HSQ has been utilized as a popular molecular precursor for Si-based nanomaterials, that is, nanocrystalline Si/SiO₂ composites, Si_xGe_{1-x}, through high-temperature thermal transformation^[2, 3, 54-66] or room-temperature mechanochemical treatment^[67].

HSQ combines mechanical, thermal, and chemical stability with solution processing, simple thin-film fabrication processing, and the flexibility of soft materials. In this review, we discuss the utilization of these attributes in a diverse range of nanoscale patterning applications. In comparison with traditional lithographic resists, HSQ exhibit several advantages in terms of the mechanical and physical properties that are important for nanoscale patterning media. HSQ can be customized to showcase a wide range of functional applications that go beyond creating physical patterns as resists or sacrificial components for transferring patterns into functional materials but act as precursors for functional silicon-based nanomaterials. In this study, we focus on the application-related aspects of nanomanufacturing for integrated circuits and nanoscale patterning and review the technical applications of HSQ in the fabrication of functional silicon-based materials.

1. Interlayer dielectric and protective coating materials

In the semiconductor industry, as the feature size of devices is scaled down to the deep sub-micrometer region, the interconnection delay (i.e., resistance-capacitance delay) becomes a performance-limiting factor for ultra-large-scale integration circuits. Dielectric materials with lower dielectric constants are required to reduce wiring capacitance and improve device performance. The integration of HSQ as an interlayer dielectric in multilevel interconnects has garnered considerable attention in recent years. This class of inorganic spin-on dielectrics potentially combines the desired features of a low dielectric constant (< 3), excellent gap fill, planarization performance, non-etch back processes, and the capability of using a standard spin-on production technique, which has been reported to lower the capacitance between adjacent metal interconnects, reducing electrical delay and increasing the information processing rate of the device^[9, 10, 68-78]. Curing is a significant process during the backend of the line fabrication of integrated circuits because it affects the structure and properties of the spin on the dielectric

material. However, both the leakage current and the dielectric constant of HSQ increase rapidly as the film being treated in temperatures higher than 400 °C^[79-82]. Furthermore, based on an experimental investigation of thermal curing, the following possible reactions were proposed^[77, 80-81, 83-86]:



At a temperature of less than 200 °C, the removal of the residual solvent was performed. In the ranges of 250–350 and 350–450 °C, the predominant reactions are expressed in Equations 1–3 and 4, respectively, with SiH₄ and H₂ being the main product. At temperatures higher than 450 °C, SiH₄ evolution decreased, and H₂ was formed. This formation could be the result of the thermal decomposition of SiH₄ in the gas phase under inert conditions, as expressed in Equation 5. Traces of oxygen promoted the oxidation of SiH₄, as shown in the last step. The unusual thermal curing behavior of the HSQ films is reflected in their physical properties. Bremmer et al. reported temperatures of 400 °C or higher resulted in increased dielectric constant and film stress^[81]. In addition to the curing temperature, the curing time and atmospheric process parameters also affect the structure and properties of HSQ films. To enhance the thermal stability of low-dielectric-constant HSQ, ion implantation^[87], H₂ plasma pretreatments^[70, 88, 89], metal composition (Cu, Ti, Ta, TiN, and TaN), barrier layer^[90-92] deposition, and optimized process conditions^[93] have been widely studied.

In protective coatings, HSQ acts as an isolated matrix to protect Si fins for advanced multiple-gate MOSFETs (Fig. 2-a), exhibiting excellent planarization and gap fill capabilities^[94]. Moreover, HSQ has also been investigated as a passivation layer in thin-film transistor liquid crystal displays, as shown in Fig. 2-b, which not only lowers the resistive-capacitive time delay in the device but also enhances the brightness of the displays^[95, 96].

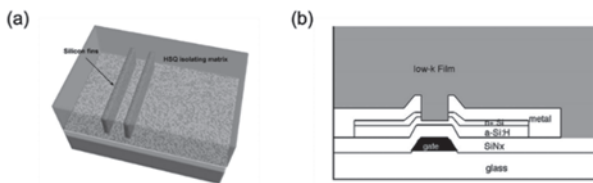


Figure 2. (a) Picture of HSQ matrix covering the silicon fins for a multi-gated MOSFET process (reprinted from Appl. Surf. Sci., 2006, 253, 395-399. Copyright © 2006 Elsevier B.V.). (b) The schematic of BCE a-Si:H TFT passivated by HSQ (low-k film) (reprinted from Thin Solid Films, 2006, 498, 70-74. Copyright © 2006 Elsevier B.V.).

2. Application in nanoscale lithography

Lithography is a process used in the semiconductor industry to create a desired pattern in a resist layer and the subsequent transfer of that pattern into or onto the underlying substrate. The basic steps of the lithographic process are schematically illustrated in Fig. 3, including coating, exposure, development, and pattern transfer, such as lift-off or etching^[24]. The lithography process is critical in the production of semiconductor devices because it determines the size and shape of the circuits printed onto the substrate. As circuit designs have become increasingly complex and the demand for smaller and more powerful chips increased, lithography technology had to keep pace with the need for ever-

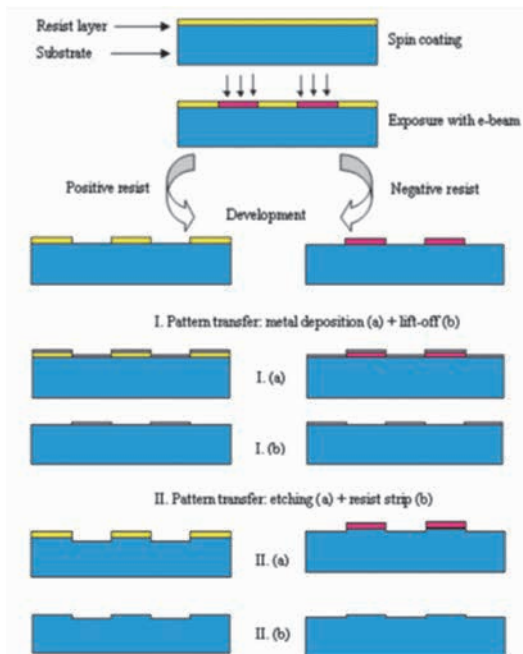


Figure 3. Schematic representation of the basic steps of a lithographic process including coating, exposure, development and pattern transfer such as lift-off or etching. (Reprinted from Nanotechnology, 2009, 20, 292001. Copyright © 2009 IOP Publishing).

smaller nanoscale feature sizes. Currently, the most advanced lithography systems can produce features as small as a few nanometers^[28], allowing the creation of complex integrated circuits with billions of transistors. Owing to its intrinsic capacity for patterning, HSQ is widely utilized in lithography and other applications that incorporate or require nanoscale patterns. This study investigated the utilization of HSQ as an inorganic negative-tone resist for various lithographies, including EBL, EUV lithography, nanoimprint lithography, step and flash imprint lithography, and masking in dry-etching processes.

2.1 EBL resist

In 1998, a 20-nm wide negative HSQ resist with a rectangular cross-sectional shape for EBL was first reported by Namatsu et al^[5]. Fig. 4-a shows a SEM image of the HSQ patterns. The HSQ resist films were spin-coated onto silicon wafers using flowable oxide, a commercially available HSQ solution manufactured by the Dow Corning Corporation (Midland, MI, USA), and subsequently baked and exposed to an electron beam to

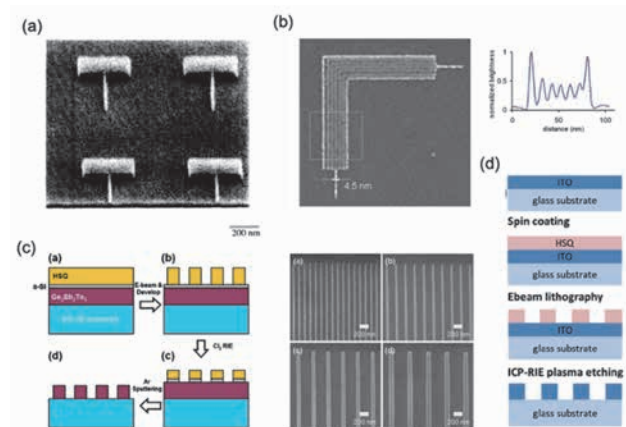


Figure 4. (a) SEM image of HSQ patterns (Reprinted from Microelectron. Eng., 1998, 41/42, 331-334. Copyright ©1998 Elsevier Science B.V.). (b) SEM image of 4.5-nm-half-pitch nested-L structures patterned in 10-nm-thick HSQ at 10 kV acceleration voltage (Reprinted from J. Vac. Sci. Technol. B, 2009, 27, 2622. Copyright © 2009 American Vacuum Society). (c) Left: schematic flow chart of suggested patterning procedure of $\text{Ge}_2\text{Sb}_2\text{Te}_5$ film. Right: HSQ line arrays with widths of a-40, b-60, c-80, and d-100 nm on an a-Si/ $\text{Ge}_2\text{Sb}_2\text{Te}_5$ /oxide substrate (reprinted from J. Electrochem. Soc., 2007, 154, H844-H847. Copyright © 2007 The Electrochemical Society). (d) Schematic of the fabrication procedure of ITO photonic crystal using e-beam patterned HSQ resist (reprinted from J. Vac. Sci. Technol. B, 2020, 38, 022802. Copyright © 2020 American Vacuum Society).

withstand subsequent processing, typically developed in an aqueous alkali solution such as tetramethyl ammonium hydroxide. They suggested that the reaction mechanism of the HSQ resist was based on two steps: (1) Si–H bonds were broken during electron beam irradiation and converted to silanol groups in the presence of absorbed moisture, and (2) unstable silanol groups were crosslinked to form a linear network. HSQ was employed as a single layer, allowing dense lines and spaces with a resolution as small as 20 nm and single lines with widths as small as 15 nm were established by Falco et al.^[16] The limiting factors of the EBL resolution include spot size, electron scattering, secondary electron range, resist development, and mechanical stability of the resist^[97]. In general, the patterning resolution can be improved by reducing the width of the electron-beam exposure point-spread function and increasing the resist contrast, which can also enhance the density of nanopatterning^[98-105]. By refining the exposure strategies, development procedures, and reducing the film thickness, high-resolution isolated lines measuring 6 nm in width and gratings with periodicities as small as 27 nm were reported^[17]. Namatsu et al.^[18] accurately measured the diameter of a well-configured electron beam as 3.6 nm. Using this fine beam, they successfully formed patterns that were 5–6 nm wide in the HSQ resist at the center and corners of the main deflection field. However, the minimum electron beam point spread function is not always easily modified. For instance, smaller point-spread functions can be achieved using high electron-beam acceleration voltages. Manfrinato et al. reported that a 200 keV EBL with an aberration-corrected STEM can be used to pattern 2 nm isolated features and 5 nm half-pitch structures in HSQ^[28]. The dependence of the contrast enhancement on the concentration and type of cations and anions in the aqueous developer solution was observed. Contrast values as high as 10 in a 115-nm-thick resist were achieved by developing HSQ in an aqueous mixture of NaOH alkali and NaCl salt^[21]. The improved contrast of HSQ enabled the fabrication of 7 nm half-pitch nested-“L” structures in a 35 nm-thick resist using a 30 kV electron-beam acceleration voltage. Subsequently, Berggren et al.^[23] demonstrated the patterning of 4.5 nm half-pitch structures (Fig. 4-b) using EBL exposure combined with a high-contrast salty solution development process.

It is easy to understand that EBL provides excellent patterning resolution with the resist of HSQ in

nanotechnology research and development of nanoscale semiconductor devices^[19, 106-116] and biodevices^[117, 118]. Baek et al. developed HSQ resist trimming and hybrid lithography techniques to scale down gate-line patterns to sub-10 nm with high accuracy and reproducibility^[19]. Using this novel process, triple-gate MOSFETs with a gate length of 6 nm were successfully fabricated. Although the length of this device is extremely small, its operational characteristics exhibit excellent performance, such as, a good subthreshold slope and large on/off current ratio. A fabrication process based on HSQ resist has the potential to produce high-performance silicon-on-insulator-based photonic wire device structures owing to the high resolution and etch resistance of HSQ, which allows direct masking of the silicon core^[108]. Moreover, HSQ acts as a sacrificial part; in other words, a mask for transferring patterns onto functional materials has been reported^[106, 107, 116]. Nam et al. demonstrated the successful electron-beam patterning of Ge₂Sb₂Te₅ nanostructures in the form of lines and dots using an HSQ resist^[107]. The fabrication process is shown in Fig. 4-c, where the patterns were transferred using a two-step etching process, in which Cl₂ and Ar were used in each step. HSQ was used as a high-resolution EBL resist to pattern Ge₂Sb₂Te₅ nanostructures with feature sizes as small as 40 nm. To improve the light extraction and quality factor cavity applications of organic light-emitting diodes, EBL was used for ITO patterning. A technological process for fabricating photonic crystals in the ITO layer in the visible range was developed using an electron-beam-patterned HSQ resist, as illustrated in Fig. 4-d^[116]. In this study, owing to its high resistance and mechanical strength, a high-resolution patterned HSQ resist was used as a mask to transfer photonic crystal nanostructures to a 150 nm-thick ITO layer. For biodevices, the use of electron-beam-patterned HSQ resists in the fabrication of triangular nanochannels for deoxyribonucleic acid (DNA) analysis, drug delivery^[117], and solid supports for light-directed in situ ssDNA synthesis^[118] have been introduced.

2.2 EUV lithography resist

EUV lithography at a wavelength of 13.5 nm has proven to be a promising solution to meet the resolution requirements of the microelectronics industry, particularly for the production of high-density features with critical dimensions of 45 nm and below. Nealey et al.^[29] reported that HSQ has a sensitivity of 11.5 mJ/cm² with a contrast of 1.64 in EUV exposure and is able to

resolve 26 nm dense lines in ~ 70 nm thick film with a low line edge roughness of 5.1 nm, indicating that HSQ exhibit distinct advantages over traditional chemically amplified resists for application in EUV lithography. Stefan et al. presented EUV lithography on an HSQ resist at resolutions of 16 and 22 nm by adding silanol or carbinol (R-CH₃OH) groups to partially cross-linked HSQ cages to increase its tetramethylammonium hydroxide developer and EUV sensitivity^[30]. They reported that to achieve high-resolution, high-volume manufacturing via EUV lithography, additional refinements to the HSQ-based system are required to surmount the developer solubility and dose trade-off, which is still under investigation. HSQ patterns with a half-pitch as small as 20 nm and linewidths as small as 10 nm using EUV interference lithography have been reported^[31]. This resolution was achieved through the development of high-concentration developers for long development times, which is in line with previous results obtained with EBL. Sub-10 nm half-pitch resolution using an HSQ resist has been reported^[32].

EUV interference lithography uses diffracted, coherent light beams to create high-resolution patterns. However, creating the necessary diffraction grating masks through EBL is limited by the electron proximity effect and pattern transfer issues. To overcome these limitations, a team of researchers patterned HSQ lines at a relaxed pitch and used conformal iridium deposition via atomic layer deposition to create diffraction gratings, resulting in a 6 nm half-pitch pattern^[119]. Winter et al. reported that EUV could be used to create periodic patterns on 1-nm thick carbon nanomembranes and single-layer graphene with sizes ranging from 20 to 500 nm, as illustrated in Fig. 5-a^[120]. The resulting nanosheets and nanoribbons can be made into supported films or freestanding objects on holey supports and grids (Fig. 5-b). In this study, HSQ was employed as a standard negative photoresist in high-resolution lithography to fabricate nanoribbon patterns with widths as small as ~ 20 nm in carbon nanomembranes. HSQ has also been used as an EUV resist in etching-mask applications for the synthesis of metal nanoparticle arrays^[121, 122], nanowires, and nanodots^[123] packed over large areas.

2.3 Proton beam writing resist

Although HSQ is primarily used as a high-resolution negative-tone electron beam resist, it is also expected to exhibit negative-tone behavior for photon beam exposures. HSQ is a superior resist for p-beam writing,

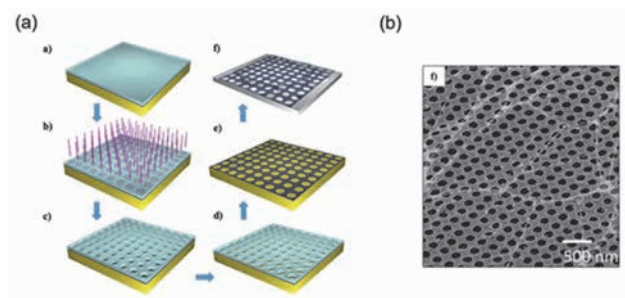


Figure 5. (a) Schematic of the nanopatterning process based on EUV-IL. (a:a) The 2D material (black) on a substrate (yellow, Au) is spin-coated with a photoresist layer. (a:b) The photoresist is irradiated with the EUV interference pattern and subsequently developed (a:c). Thereafter, the structure is induced into the underlying material via RIE (a:d). Finally, the photoresist is dissolved (a:e). The structure can subsequently be transferred onto a holey substrate (a:f) to prepare a self-supporting, perforated sheet or an array of nanoribbons. (b) Freestanding graphene monolayers on holey lacey carbon support films: graphene nano-mesh with 175 ± 5 nm wide openings and 90 ± 5 nm wide graphene features on an area of $50 \mu\text{m} \times 50 \mu\text{m}$ (reprinted from 2D Mater., 2019, 6, 021002. Copyright © 2019 IOP Publishing Ltd).

allowing the production of high-aspect-ratio structures as small as 22 nm^[37]. HSQ shows great potential for proton-beam writing in three-dimensional (3D) nanolithography^[38]. Using HSQ as a resist, it has been possible to directly write details with a width as small as 20 nm and a height of 850 nm. Proton beam writing with HSQ provides a new method for creating high-density 3D nanostructures with reduced proximity effects compared with the widely adopted e-beam writing technique.

2.4 Molding material in nanoimprint lithography

Nanoimprint lithography is an attractive method for achieving high-resolution pattern replication at a low cost and high throughput. This process involves the physical deformation of a heated polymer coated on a silicon substrate using a mold deposited on the substrate. The resulting resist pattern is thereafter subjected to reactive ion etching to create a useful profile for the subsequent hard material pattern transfer. HSQ has been successfully used as a mold owing to its strong adhesion to silicon substrates and structural similarity to SiO₂ after thermal or electron-beam curing^[39, 40]. Room-temperature nanoimprint lithography without a resist thermal cycle or UV exposure using HSQ was also reported by Matsui et al^[42-47].

Gold nanoparticle (Au NP) patterns fabricated using

imprinted HSQ patterns for surface-enhanced Raman scattering (SERS) was first reported by Matsui et al.^[124]. The successful assembly of the negatively charged Au NPs followed the geometry of the negatively charged HSQ pattern. Moreover, a comparison between substrates fabricated using an inorganic polymer (HSQ) and an organic polymer demonstrated that the SERS substrate fabricated from HSQ was well suited for organic chemical analysis.

2.5 Step and flash imprint lithography resist

Step and flash imprint lithography is a variation of nanoimprint lithography that uses a UV-transparent template with a relief image to replicate patterns, and is performed at room temperature and low pressure. This involves coating the wafers with an organic polymer transfer layer, pressing the template into the layer, curing the resist, removing the template, performing a fluorocarbon reactive ion etching step to remove the polymer layer residues, and performing oxygen etching to transfer the pattern to the substrate. In their study, Mancini et al. explored the use of HSQ for direct electron-beam patterning of step and flash imprint lithography templates^[48]. They coated quartz photomask substrates with an ITO charge-dissipation layer and patterned them with an electron beam using a 100 nm thick HSQ resist layer. The highest resolutions of 20 and 30 nm were achieved on the templates and imprinted wafers, respectively (Fig. 6).

2.6 Mask in dry etching processes

As previously discussed in the EBL resist section, HSQ is a promising material for negative resist in nanopatterning and hard mask during dry etching owing to the nanoscale device fabrication because of its high resolution, high etching resistance, and compatibility with various substrate materials^[106, 107, 116]. Moreover, the

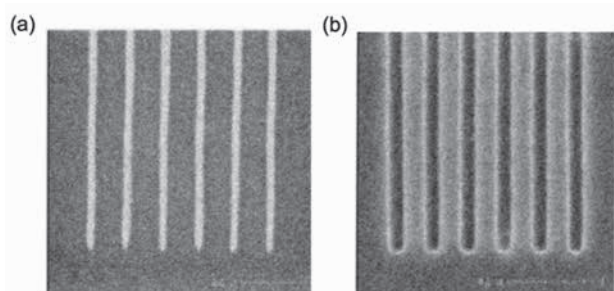


Figure 6. Top down SEM of lines down at 25 and 30 nm pitch resolutions written with SFIL on (a) templates and (b) imprinted wafers (reprinted from J. Vac. Sci. Technol. B, 2002, 20, 2896. Copyright © 2002 American Vacuum Society).

utilization of HSQ as a resist in the nanopatterning process and as a mask in the dry etching process has also been developed for the fabrication of MOSFET gates with an even 6 nm gate length^[19, 125], low-loss nanowires in silicon-on-insulator (Fig. 7)^[108], sub-micron GaAs^[49], sub-10 nm features into metal^[126], and metallic nanostructures for nanophotonic and plasmonic^[127].

3. Molecular precursors for silicon-based nanomaterials

Semiconductor materials composed of group IV elements have been intensely studied for a broad range of potential applications, from photovoltaics and fluorescent contrast agents to color displays, such as the recently commercialized quantum dot light-emitting diode displays. In this section, HSQ is introduced as the precursor of oxide-embedded and freestanding Si-containing group IV semiconductor nanomaterials with well-defined sizes and optical properties, such as photoluminescence (PL) and quantum yield (QY).

3.1 Oxide-embedded and freestanding silicon nanocrystals (Si NCs)

In 2006, the first preparation of nanocrystalline Si-SiO₂ composites via thermal pyrolysis of a well-defined molecular HSQ precursor was reported by Veinot et al.^[54], as illustrated in Fig. 8-a. Si NCs-embedded SiO₂ started to be observed after one-hour thermal pyrolysis of HSQ at temperatures higher than 800 °C under a mixed inert atmosphere of 4% H₂ and 96% N₂. The size of the Si NCs can be tuned by controlling the annealing temperature and/or time. Si NCs with a size of 3.3 nm can be obtained at temperatures close to 1100 °C, which

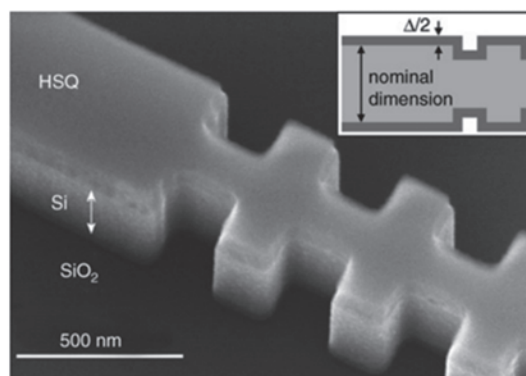


Figure 7. SEM image of a photonic wire Bragg grating fully etched into silicon waveguide core layer with HSQ as an EBL resist and mask (reprinted from Electron. Lett., 2008, 44, 115-116. Copyright © 2008 The Institution of Engineering and Technology).

increased to 9 nm as the temperature increased to 1400 °C. An increase in size was also observed with an increase in the annealing time^[56]. The formation of oxide-embedded Si NCs through the thermal pyrolysis of HSQ in a reducing atmosphere (i.e., 96% N₂ or Ar and 4% H₂) has been identified in three stages^[2, 54, 56]:

1. HSQ structural changes, including trace solvent loss (< 200 °C), cage network rearrangements with associated loss of SiH₄ (250–350 °C), Si–H thermal dissociation with the formation of SiH₄ and H₂ (350–450 °C), and HSQ cross-linking.
2. With the temperature increasing to 450 °C, rapid thermal decomposition of SiH₄ results in the formation of oxide-embedded Si nanodomains. The specific role of hydrogen in thermal processing was investigated. It is possible that low H₂ concentrations limit or even prevent the dehydrogenation of HSQ, thus increasing the amount of SiH₄ available for thermal decomposition.
3. Nanodomain crystallization and growth. At temperatures higher than 900 °C, processing temperature drives the growth and increases crystallinity of Si nanodomains, whereas prolonged heating at 1100 °C results in an annealing process that passivates volume defects.

The luminescent nanocrystalline Si/SiO₂ thin films and patterns formed after thermal pyrolysis (1100 °C) from solution processable HSQ have been reported^[128]. Free-standing Si NCs with hydrogen-terminated surfaces (H–Si NCs) can be liberated from the matrix composite

through the chemical etching of SiO₂ using hydrogen fluoride (HF), as shown in Fig. 8-b. The etching procedures have been reported in previous studies^[129]. The most significant procedure is the use of HF/hydrogen chloride, which provides faster etching. The emission of these freestanding H–Si NCs in the range of 520–750 nm depended on the etching time (Fig. 8-d). The observed blue shift in the PL maximum upon extended exposure to HF can be attributed to the quantum confinement effects arising from the decreased size. The PL and QYs of the H–Si NCs was approximately 4%. However, H–Si NCs were significantly unstable and easily oxidized because of the low disassociation bond energy of Si–H. Various surface passivation methods have been outlined in previous studies^[130-137]. Typically, the surface passivation of alkyl groups is induced through thermal-^[130, 131], photo-^[132], radical-initiated-^[133], and Lewis-acid-initiated^[135] reactions between H–Si NCs and alkenes, resulting in the formation of robust Si–C covalent bonds instead of Si–H on the surface (Fig. 8-c). Dasog et al. reported the preparation of surface-passivated Si NCs with PL across the entire visible spectral region via surface engineering with alkyl, amine, phosphine, and acetal functional groups without altering the size to 3–4 nm (Fig. 9-a)^[134]. The surface-state-dependent emission exhibited short-lived excited states and higher relative PL QYs than Si–NCs of equivalent size, which exhibited emission originating from the bandgap transition. This study highlights the importance of surface states and their crucial role in the

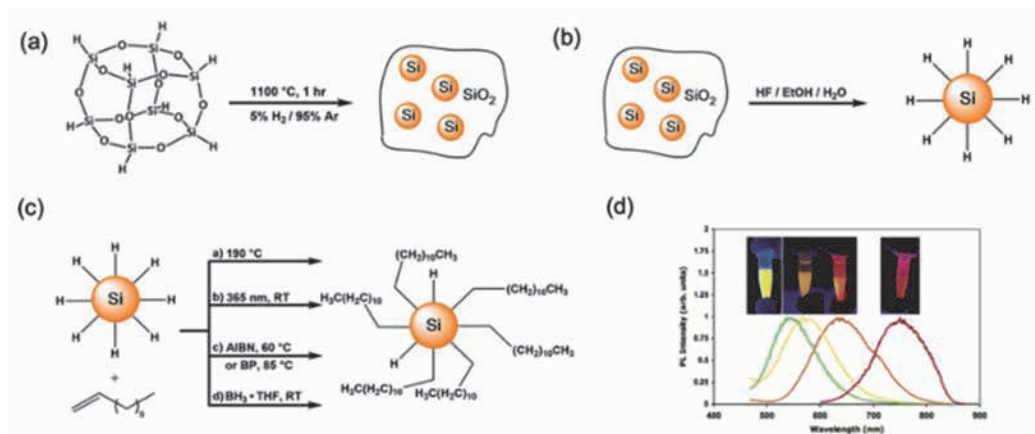


Figure 8. (a) Synthesis of oxide-embedded Si NCs through thermal pyrolysis. (b) Liberation of freestanding H–Si NCs through HF chemical etching. (c) Surface passivation of H–Si NCs by alkene via a) thermal, b) photo, c) radical initiated, and d) Lewis's acid reaction (reprinted from Chem. Mater., 2017, 29, 80-89. Copyright © 2016 American Chemical Society). (d) PL of liberating H–Si NCs by varying etching time: 50 (red), 85 (orange), 115 (yellow), and 135 minutes (green), resulting in decreased size. Inset: photographs of PL observed upon exposure to a standard handheld UV light (reprinted from Chem. Mater., 2006, 18, 6139-6146. Copyright © 2006 American Chemical Society).

optical properties of Si NCs. Subsequent studies revealed that by altering the surface ligands, the PL range could be extended to encompass the full color spectrum within the 400–800 nm wavelengths^[61-63, 138-140]. For instance, the surface passivation of Br, I, and Cl ligands, instead of hydrogen in the H–Si NCs, generates red, orange, and blue PL, respectively (Fig. 9-b)^[61]. Recent research has reported QYs reaching up to 80% in the orange-red wavelength region^[139]. Several studies have been conducted on the thermal pyrolysis of a well-defined commercial HSQ, namely, the $H_8Si_8O_{12}$ cubic cluster. Si NCs with a size of 1–10 nm have been prepared through thermal pyrolysis (1100 °C) of lab synthesized $(HSiO_{1.5})_n$ ($n > 8$) polymer with different ratios of network-to-cage structures (as shown in Fig. 9-c)^[2, 3, 141]. During the polymer synthesis process, the network-to-cage structures of the obtained molecules can be controlled by the experimental conditions, such as the species and/or amounts of chemical reagents and the reaction speed. The higher network-to-cage degree and cross-linking density exhibited by the $(HSiO_{1.5})_n$ polymer increased the energy required for Si to diffuse across the oxide matrix, resulting in the formation of smaller Si NCs. Furthermore, the freestanding Si NCs exhibited size-dependent PL in accordance with the principles of quantum confinement, with tunable PL across the visible and near-infrared (NIR) spectra and QYs ranging from 3

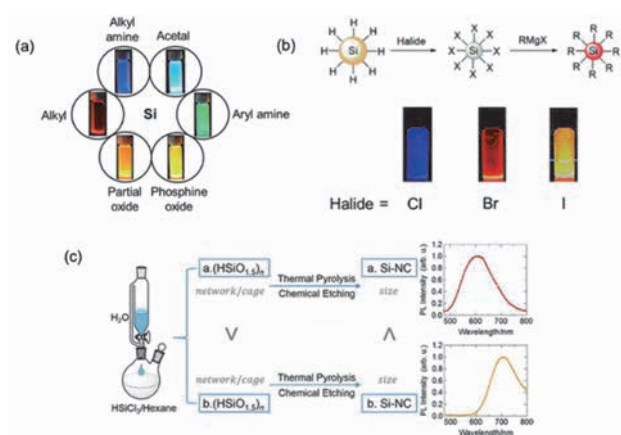


Figure 9. (a) Photograph of emissive Si NCs passivated by different functional groups (reprinted from ACS Nano, 2014, 8(9), 9636-9648. Copyright: © 2014 American Chemical Society). (b) Photograph of emissive Si NCs passivated by different Halide groups (reprinted from Chem. Mater. 2015, 27, 4, 1153-1156. Copyright © 2015 American Chemical Society). (c) Size-controlled Si NCs synthesized using the structure of selectively synthesized HSQ polymers (reprinted from Chem. Lett. 2017, 46, 5, 699-702. Copyright: © 2017 The Chemical Society of Japan).

to 10%.

In brief, to control the size of Si NCs in the aforementioned process, two alternative methods were adopted by precisely manipulating the temperature/time during thermal pyrolysis and modifying the chemical structure of the $(HSiO_{1.5})_n$ polymer. The use of cost-effective $(HSiO_{1.5})_n$ polymers as precursors for the production of Si–NCs is advantageous. However, the requirement for extremely high temperatures during thermal pyrolysis and a continuous supply of H_2 throughout the pyrolysis and cooling processes are significant drawbacks. Xu et al. demonstrated a sustainable and green alternative to conventional thermal transformations from $(HSiO_{1.5})_n$ polymers to functional Si NCs via a room-temperature mechanochemical process with zero H_2 supply^[67]. The size of the Si NCs (<10 nm) embedded in the SiO_2 matrix could be easily controlled by varying the milling ball size (ZrO_2 , 3–15 mm) and mechanochemical duration (400 rpm, 1–3 hours). The mechanism of the reaction from $(HSiO_{1.5})_n$ to Si NCs via a mechanochemical route distinct from that of conventional thermal pyrolysis is as follows (Fig. 10-a)^[67]:

1. Network structure breakage under mechanical stress, Si–H bond cleavage accompanied by formation

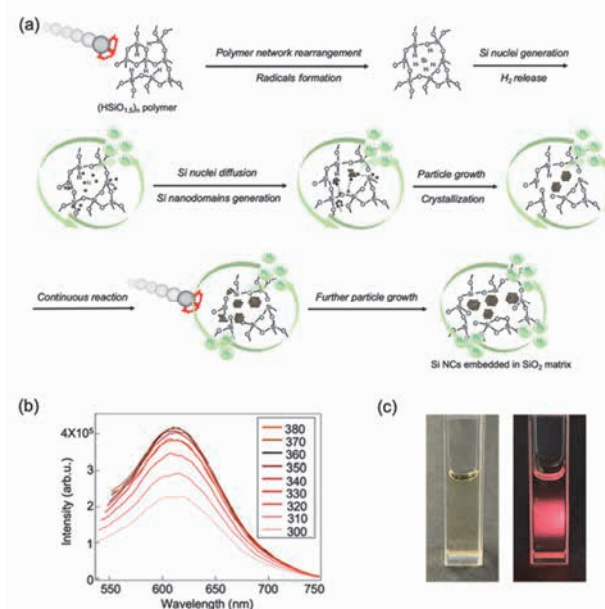


Figure 10. (a) Transformations from HSQ polymer to emissive Si NCs via a room-temperature mechanochemical process reported by Xu et al. (b) PL of free-standing alkyl-Si NCs synthesized from the mechanochemical process with milling ball in diameter of 10 mm. (c) Photographs of alkyl-Si NCs dispersion under ambient light (left) and UV light with a wavelength of 350 nm (right) (reprinted from J. Mater. Chem. C, 2022, 10, 12588. Copyright: © The Royal Society of Chemistry 2022).

- of radicals and redistribution of Si–O–Si bonds.
2. H₂ and Si nuclei generation.
3. Si nuclei diffusion and formation of Si nanodomains.
4. Particle growth and crystallization of Si nanodomains by continuously induced mechanical energy.
5. Further particle growth. With the increased reactivity of the additional polymers, the quantity and size of the Si NCs increased because of the intensified formation of Si radicals and nuclei. The amount of Si NCs was significantly increased by subsequent mechanochemical treatments.

The author stated that to achieve an efficient reaction of the (HSiO_{1.5})_n polymer, it is necessary to not only induce sufficient mechanical impact energy (determined by the size of the milling balls) but also frequent collisions (dependent on the number of milling balls) between the milling balls and the (HSiO_{1.5})_n precursor. The freestanding alkyl-passivated Si NCs exhibited bright emission in visible light region with QY of 9.8%, whose value is comparable to that synthesized by the conventional thermal pyrolysis of (HSiO_{1.5})_n precursor (Figs. 10-b and c). Moreover, when processing same amounts of (HSiO_{1.5})_n polymer, mechanochemical treatment consumed only one-fifteenth of the energy and a negligible amount of gas compared to high-temperature thermal pyrolysis (1100 °C). This novel and facile mechanochemical route opens new avenues for the smart synthesis of functional nanomaterials.

3.2 Oxide-embedded and freestanding Si_xGe_{1-x} alloy NCs (64 < x < 100)

In 2001, Veinot et al. reported the preparation of Si_xGe_{1-x} alloy NCs using HSQ and soluble germanium diiodide (GeI₂) complexes^[64]. Trialkylphosphine adducts facilitate the formation of a homogenous precursor for oxide-embedded Si_xGe_{1-x} NCs via thermal pyrolysis at 1100 °C in 1–9 hours. The freestanding passivated Si_xGe_{1-x} NCs (< 20 nm) exhibit bright NIR PL and QYs of 16 ± 3%. The GeI₂ precursor facilitated the nucleation of larger Si_xGe_{1-x} NCs. A separate population of Si-rich NCs is formed through matrix diffusion, and may also incorporate low amounts of Ge through matrix diffusion processes.

3.3 Boron (B)- and/or phosphorus (P)- doped Si NCs

For electronic applications, organic-functionalized Si NC surfaces deteriorate the carrier transport of films because of the increased NC-to-NC distance. To

overcome this problem, B- and P-doped all-inorganic Si NCs were developed^[65, 66]. Si NCs doped with B and/or P were synthesized in glass matrices using annealing solutions containing HSQ and dopant acids as illustrated in Fig. 11. Subsequently, the NCs were extracted from the matrices via HF etching. The resulting free-standing NCs exhibited dispersibility in methanol without requiring any additional surface functionalization processes because the hydrophilic shells were heavily doped with B and P on the surface of the Si NCs. The NCs exhibited size-tunable PL with high efficiency, covering a broad range from the NIR to the visible region.

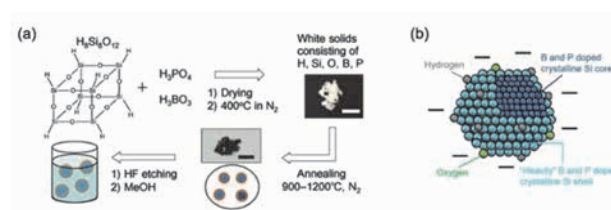


Figure 11. (a) Preparation procedure of all-inorganic B- and P-doped colloidal Si NCs. (Scale bars: 1 cm) (b) Schematic of the structure of B- and P-doped crystalline Si core (reprinted from *Nanoscale*, 2014, 6, 12354-12359. Copyright: © The Royal Society of Chemistry 2014).

In summary, HSQ is a promising dielectric material for use in integrated circuits owing to its low dielectric constant, excellent gap fill and planarization properties, and the capability to use standard spin-on production techniques. However, its thermal stability is a significant issue, as the leakage current and dielectric constant increase rapidly at temperatures higher than 400 °C. Various methods have been proposed to enhance the thermal stability of HSQ, including ion implantation, H₂ plasma pretreatment, and metal-composite barrier layer deposition. Additionally, HSQ has also been used as a protective coating and passivation layer in advanced multiple-gate MOSFETs and thin-film transistor liquid crystal displays, respectively. In lithography, HSQ has been used as a standard industrial negative-tone resist applicable for high-resolution and small linewidth fluctuations in EBL, EUV lithography, nanoimprint lithography, and step and flash imprint lithography. Sub-10-nm isolated features are now frequently obtained in HSQ and even 4.5 nm-half-pitch structures have been successfully obtained. HSQ is used as a resist in several applications, including the fabrication of MOSFET gates with a 6 nm gate length, etching masks in bilayer

lithographic processes, and imprinting templates for selective metal deposition, and step and flash imprint lithography. In addition to nanomanufacturing for photonic and electronic devices, HSQ has also been extensively reported as a precursor for fabrication of semiconductor nanomaterials, such as Si NCs and $\text{Si}_x\text{Ge}_{1-x}$, at extremely high temperatures ($\geq 1100\text{ }^\circ\text{C}$) under continuous supply of H_2 and inert atmosphere. Moreover, it is difficult to control the particle size by precisely manipulating the temperature during thermal pyrolysis and modifying the chemical structure of HSQ. A sustainable and green alternative to conventional thermal transformations from HSQ to functional Si NCs via a room-temperature mechanochemical process with zero H_2 supply was also demonstrated. Si NCs were synthesized using different methods and their sizes and optical properties were extensively studied. We demonstrated that Si NCs with a quantum-confinement-effect-induced unique electronic structure and optical properties hold great promise for applications in next-generation optoelectronic devices^[57, 140, 142-144], photovoltaic^[145-147], and in vivo and in vitro bio-imaging^[148-150]. Overall, HSQ is a versatile and valuable material with a wide range of applications in nanomanufacturing and nanofabrication. As technology continues to advance, the use of HSQ is expected to become increasingly important in the development of new and innovative nanoscale devices and functional semiconductor materials.

[References]

- [1] Frye, C. L.; Collins, W. T., *J. Amer. Chem. Soc.*, **92**, pp.5586-5588 (1970).
- [2] Henderson, E. J., Kelly, J. A., Veinot, J. G. C., *Chem. Mater.*, **21(22)**, pp.5426-5434 (2009).
- [3] Xin, Y., Wakimoto, R., Saitow, K. I., *Chem. Lett.*, **46(5)**, pp.699-702 (2017).
- [4] Albrecht, M. G., Blanchette, C., *J. Electrochem. Soc.*, **145(11)**, pp.4019 (1998).
- [5] Namatsu, H., Takahashi, Y., Yamazaki, K., Yamaguchi, T., Nagase, M., Kurihara, K., *J. Vac. Sci. Technol., B: Microelectron. Nanometer Struct. Process., Meas., Phenom.*, **16(1)**, pp.69-76 (1998).
- [6] van Delft, F. C., Weterings, J. P., van Langen-Suurling, A. K., Romijn, H., *J. Vac. Sci. Technol., B: Microelectron. Nanometer Struct. Process., Meas., Phenom.*, **18(6)**, pp.3419-3423 (2000).
- [7] Mollard, L., Cunge, G., Tedesco, S., Dal'zotto, B., Foucher, J., *Microelectron Eng.*, **61**, pp.755-761 (2002).
- [8] Henschel, W., Georgiev, Y. M., Kurz, H., *J. Vac. Sci. Technol., B: Microelectron. Nanometer Struct. Process., Meas., Phenom.*, **21(5)**, pp.2018-2025 (2003).
- [9] K. D. Weiss, C. L. Frye, Patent US4999397 (1991).
- [10] H. M. Bank, M. E. Ciufentes, T. E. Martin, Patent US5010159 (1991).
- [11] Chandra, G., *MRS Online Proceedings Library (OPL)*, **203**, pp.97-108 (1990).
- [12] Loboda, M. J., Grove, C. M., Schneider, R. F., *J. Electrochem. Soc.*, **145(8)**, pp.2861 (1998).
- [13] Liu, P. T., Chang, T. C., Tsai, T. M., Lin, Z. W., Chen, C. W., Chen, B. C., Sze, S. M., *Appl. Phys. Lett.*, **83(20)**, pp.4226-4228 (2003).
- [14] Namatsu, H., Nagase, M., Yamaguchi, T., Yamazaki, K., Kurihara, K., *J. Vac. Sci. Technol., B: Microelectron. Nanometer Struct. Process., Meas., Phenom.*, **16(6)**, pp.3315-3321 (1998).
- [15] Do, H. W., Chang, J. B., Berggren, K. K., *J. Vac. Sci. Technol., B*, **32(6)**, pp.06F501 (2014).
- [16] van Delft, F. C., Weterings, J. P., van Langen-Suurling, A. K., Romijn, H., *J. Vac. Sci. Technol., B: Microelectron. Nanometer Struct. Process., Meas., Phenom.*, **18(6)**, pp.3419-3423 (2000).
- [17] Word, M. J., Adesida, I., Berger, P. R., *J. Vac. Sci. Technol., B: Microelectron. Nanometer Struct. Process., Meas., Phenom.*, **21(6)**, pp.L12-L15 (2003).
- [18] Yamazaki, K., Namatsu, H., *Jpn. J. Appl. Phys.*, **43(6B)**, pp.3767-3771 (2004).
- [19] Baek, I. B., Yang, J. H., Cho, W. J., Ahn, C. G., Im, K., Lee, S., *J. Vac. Sci. Technol., B: Microelectron. Nanometer Struct. Process., Meas., Phenom.*, **23(6)**, pp.3120-3123 (2005).
- [20] Matsubara, Y., Taniguchi, J., Miyamoto, I., *Jpn. J. Appl. Phys.*, **45(6S)**, pp.5538 (2006).
- [21] Yang, J. K., Berggren, K. K., *J. Vac. Sci. Technol., B: Microelectron. Nanometer Struct. Process., Meas., Phenom.*, **25(6)**, pp.2025-2029 (2007).
- [22] Ocola, L. E., Tirumala, V. R., *J. Vac. Sci. Technol., B: Microelectron. Nanometer Struct. Process., Meas., Phenom.*, **26(6)**, pp.2632-2635 (2008).
- [23] Yang, J. K., Cord, B., Duan, H., Berggren, K. K., Klingfus, J., Nam, S. W., Kim, K. B., Rooks, M. J., *J. Vac. Sci. Technol., B: Microelectron. Nanometer Struct. Process., Meas., Phenom.*, **27(6)**, pp.2622-2627 (2009).
- [24] Grigorescu, A. E., Hagen, C. W., *Nanotechnology*, **20(29)**, 292001 (2009).
- [25] Vila-Comamala, J., Gorelick, S., Guzenko, V. A., Färm, E., Ritala, M., David, C., *Nanotechnology*, **21(28)**, pp.285305 (2010).

- [26] Manfrinato, V. R., Cheong, L. L., Duan, H., Winston, D., Smith, H. I., Berggren, K. K., *Microelectron. Eng.*, **88(10)**, pp.3070-3074 (2011).
- [27] Vila-Comamala, J., Gorelick, S., Guzenko, V. A., David, C., *J. Vac. Sci. Technol., B*, **29(6)**, pp.06F301 (2011).
- [28] Manfrinato, V. R., Zhang, L., Su, D., Duan, H., Hobbs, R. G., Stach, E. A., Berggren, K. K., *Nano Lett.*, **13(4)**, pp.1555-1558 (2013).
- [29] Junarsa, I., Stoykovich, M. P., Nealey, P. F., Ma, Y., Cerrina, F., Solak, H. H., *J. Vac. Sci. Technol., B: Microelectron. Nanometer Struct. Process., Meas., Phenom.*, **23(1)**, pp.138-143 (2005).
- [30] Rathore, A., Pollentier, I., Cipriani, M., Singh, H., De Simone, D., Ingolfsson, O., De Gendt, S., *ACS Appl. Polym. Mater.*, **3(4)**, pp.1964-1972 (2021).
- [31] Ekinci, Y., Solak, H. H., Padeste, C., Gobrecht, J., Stoykovich, M. P., Nealey, P. F., *Microelectron. Eng.*, **84(5-8)**, pp.700-704 (2007).
- [32] Ekinci, Y., Vockenhuber, M., Hojeij, M., Wang, L., Mojarad, N., *Proc. Extreme Ultraviolet (EUV) Lithography IV*, 8679, pp.867910 (2013).
- [33] Mojarad, N., Gobrecht, J., Ekinci, Y., *Sci. Rep.*, **5(1)**, pp.1-7 (2015).
- [34] Desai, V., Mellish, M., Bennett, S., Cady, N. C., *J. Vac. Sci. Technol. B*, **35(2)**, pp.021603 (2017).
- [35] Kim, J., Lee, J. K., Chae, B., Ahn, J., Lee, S., *Nano Converg.*, **9(1)**, pp.1-10 (2022).
- [36] Anderson, C. N., Naulleau, P. P., *J. Vac. Sci. Technol., B: Microelectron. Nanometer Struct. Process., Meas., Phenom.*, **27(1)**, pp.6-10 (2009).
- [37] Van Kan, J. A., Bettioli, A. A., Watt, F., *Nano Lett.*, **6(3)**, pp.579-582 (2006).
- [38] van Kan, J. A., Bettioli, A. A., Watt, F., *Nucl. Instrum. Methods Phys. Res. B: Beam Interact. Mater. At.*, **260(1)**, pp.396-399 (2007).
- [39] Nakamatsu, K. I., Watanabe, K., Tone, K., Namatsu, H., Matsui, S., *J. Vac. Sci. Technol., B: Microelectron. Nanometer Struct. Process., Meas., Phenom.*, **23(2)**, pp.507-512 (2005).
- [40] Nakamatsu, K. I., Matsui, S., *Jpn. J. Appl. Phys.*, **45(21)**, pp.L546-L548 (2006).
- [41] Chen, S. Z., Liu, J. F., Chen, H. J., Huang, F. S., *J. Vac. Sci. Technol., B: Microelectron. Nanometer Struct. Process., Meas., Phenom.*, **24(4)**, pp.1934-1940 (2006).
- [42] Nakamatsu, K. I., Ishikawa, K., Taneichi, N., Matsui, S., *Jpn. J. Appl. Phys.*, **46(8A)**, pp.5388-5390 (2007).
- [43] Matsui, S., Igaku, Y., Ishigaki, H., Fujita, J., Ishida, M., Ochiai, Y., Komuro, M., *J. Vac. Sci. Technol., B: Microelectron. Nanometer Struct. Process., Meas., Phenom.*, **21(2)**, pp.688-692 (2003).
- [44] Okada, M., Nakamatsu, K. I., Iwasa, M., Kanda, K., Haruyama, Y., Matsui, S., *Appl. Phys. Express*, **2(1)**, pp.016502 (2008).
- [45] Kang, Y., Okada, M., Nakamatsu, K. I., Haruyama, Y., Kanda, K., Matsui, S., *J. Photopolym. Sci. Technol.*, **22(2)**, pp.193-194 (2009).
- [46] Kang, Y., Okada, M., Minari, C., Kanda, K., Haruyama, Y., Matsui, S., *Jpn. J. Appl. Phys.*, **49(6S)**, pp.06GL13 (2010).
- [47] Kang, Y., Okada, M., Omoto, S., Haruyama, Y., Kanda, K., Matsui, S., *J. Vac. Sci. Technol., B*, **29(6)**, pp.06FC03 (2011).
- [48] Mancini, D. P., Gehoski, K. A., Ainley, E., Nordquist, K. J., Resnick, D. J., Bailey, T. C., Willson, C. G., *J. Vac. Sci. Technol., B*, **20(6)**, pp.2896-2901 (2002).
- [49] Lauvernier, D., Garidel, S., Legrand, C., Vilcot, J. P., *Microelectron. Eng.*, **77(3-4)**, pp.210-216 (2005).
- [50] Larrieu, G., Dubois, E., *J. Vac. Sci. Technol., B: Microelectron. Nanometer Struct. Process., Meas., Phenom.*, **23(5)**, pp.2046-2050 (2005).
- [51] Yang, J. K., Anant, V., Berggren, K. K., *J. Vac. Sci. Technol., B: Microelectron. Nanometer Struct. Process., Meas., Phenom.*, **24(6)**, pp.3157-3161 (2006).
- [52] O'Faolain, L., Kotlyar, M. V., Tripathi, N., Wilson, R., Krauss, T. F., *J. Vac. Sci. Technol., B: Microelectron. Nanometer Struct. Process., Meas., Phenom.*, **24(1)**, pp.336-339 (2006).
- [53] Sun, J., Iwasaki, T., Muruganathan, M., Mizuta, H., *Appl. Phys. Lett.*, **106(3)**, pp.033509 (2015).
- [54] Hessel, C. M., Henderson, E. J., Veinot, J. G. C., *Chem. Mater.*, **18(26)**, 6139-6146 (2006).
- [55] Veinot, J. G. C., *Chem. Comm.*, pp.4160-4168 (2006).
- [56] Hessel, C. M., Henderson, E. J., Veinot, J. G. C., *J. Phys. Chem. C*, **111(19)**, pp.6956-6961 (2007).
- [57] Xu, Y., Terada, S., Xin, Y., Ueda, H., Saitow, K. I., *ACS Appl. Nano Mater.*, **5(6)**, pp.7787-7797 (2022).
- [58] Kelly, J. A., Henderson, E. J., Veinot, J. G. C., *Chem. Comm.*, **46(46)**, pp.8704-8718 (2010).
- [59] Hessel, C. M., Reid, D., Panthani, M. G., Rasch, M. R., Goodfellow, B. W., Wei, J., Korgel, B. A., *Chem. Mater.*, **24(2)**, pp.393-401 (2012).
- [60] Mastronardi, M. L., Maier-Flaig, F., Faulkner, D., Henderson, E. J., Kübel, C., Lemmer, U., Ozin, G. A., *Nano Lett.*, **12(1)**, pp.337-342 (2012).
- [61] Dasog, M., Bader, K., Veinot, J. G. C., *Chem. Mater.*, **27(4)**, pp.1153-1156 (2015).
- [62] Yu, Y.; Rowland, C. E.; Schaller, R. D.; Korgel, B. A., *Langmuir*, **31**, pp.6886-6893 (2015).
- [63] Clark, R. J., Aghajamali, M., Gonzalez, C. M., Hadadi, L., Islam, M. A., Javadi, M., Mobarok, M. H., Purkait, T. K., Robidillo, C. J. T., Sinelnikov, R., Thiessen, A. N.,

- Washington, J., Yu, H., Veinot, J. G. C., *Chem. Mater.*, **29**, pp.80-89 (2017).
- [64] Barry, S. D., Yang, Z., Kelly, J. A., Henderson, E. J., Veinot, J. G. C., *Chem. Mater.*, **23(22)**, pp.5096-5103 (2011).
- [65] Milliken, S., Cui, K., Klein, B. A., Cheong, I. T., Yu, H., Michaelis, V. K., Veinot, J. G. C., *Nanoscale*, **13(43)**, pp.18281-18292 (2021).
- [66] Sugimoto, H., Fujii, M., Imakita, K. *Nanoscale*, **6(21)**, pp.12354-12359 (2014).
- [67] Xu, Y., Xin, Y., Kato, K., Shirai, T., *J. Mater. Chem. C*, **10(35)**, pp.12588-12601 (2022).
- [68] Loboda, M. J., Toskey, G. A., *Solid State Technol.*, **41(5)**, pp.99-103 (1998).
- [69] Kohl, A. T., Mimna, R., Shick, R., Rhodes, L., Wang, Z. L., Kohl, P. A., *Electrochem. Solid-State Lett.*, **2(2)**, pp.77 (1998).
- [70] Chang, T. C., Liu, P. T., Shih, F. Y., Szea, S. M., *Electrochem. Solid-State Lett.*, **2(8)**, pp.390 (1999).
- [71] Albrecht, M. G., Blanchette, C., *J. Electrochem. Soc.*, **145(11)**, pp.4019 (1998).
- [72] Chen, W. C., Lin, S. C., Dai, B. T., Tsai, M. S., *J. Electrochem. Soc.*, **146(8)**, pp.3004 (1999).
- [73] Devine, R. A. B., *J. Appl. Phys.*, **92(6)**, pp.3162-3168 (2002).
- [74] Toivola, Y., Thurn, J., Cook, R. F., *J. Electrochem. Soc.*, **149(3)**, pp.F9 (2002).
- [75] Costescu, R. M., Bullen, A. J., Matamis, G., O'Hara, K. E., Cahill, D. G., *Phys. Rev. B*, **65(9)**, pp.094205 (2002).
- [76] Cheng, Y. Y., Kan, J. Y., Lin, I. S., *Thin Solid Films*, **462**, pp.297-301 (2004).
- [77] Volksen, W., Miller, R. D., Dubois, G., *Chem. Rev.*, **110(1)**, pp.56-110 (2010).
- [78] Al-Moathin, A., Hou, L., Ofiare, A., Wang, J., Ye, S., Li, C., Marsh, J. H., *J. Vac. Sci. Technol., B: Microelectron. Nanometer Struct. Process., Meas., Phenom.*, **37(6)**, pp.061210 (2019).
- [79] Sun, S. C., Chuang, Y. C., *Proc. VLSI Multilevel Interconnection Conference (VMIC)*, pp.113 (1996).
- [80] Többen, D., Weigand, P., Shapiro, M. J., Cohen, S. A., *MRS Online Proceedings Library*, **443**, pp.195-200 (1996).
- [81] Bremme, J. N., Liu, Y., Gruszynski, K. G., Dall, F. C., *MRS Online Proceedings Library*, **476**, pp.37-44 (1997).
- [82] Chung, S. W., Shin, J. H., Park, N. H., Park, J. W., *Jpn. J. Appl. Phys.*, **38(9R)**, pp.5214 (1999).
- [83] Albrecht, M. G., Blanchette, C., *J. Electrochem. Soc.*, **145(11)**, pp.4019 (1998).
- [84] Siew, Y. K., Sarkar, G., Hu, X., Hui, J., See, A., Chua, C. T., *J. Electrochem. Soc.*, **147(1)**, pp.335 (2000).
- [85] Belot, V., Corriu, R., Leclercq, D., Mutin, P. H., Vioux, A., *Chem. Mater.*, **3(1)**, pp.127-131 (1991).
- [86] Loboda, M. J., Grove, C. M., Schneider, R. F., *J. Electrochem. Soc.*, **145(8)**, pp.2861 (1998).
- [87] Chang, T. C., Chou, M. F., Mei, Y. J., Tsang, J. S., Pan, F. M., Wu, W. F., Huang, H. D. *Thin Solid Films*, **332(1-2)**, pp.351-355 (1998).
- [88] Liu, P. T., Chang, T. C., Sze, S. M., Pan, F. M., Mei, Y. J., Wu, W. F., Huang, H. D., *Thin Solid Films*, **332(1-2)**, pp.345-350 (1998).
- [89] Chang, T. C., Liu, P. T., Shih, F. Y., Szea, S. M., *Electrochem. Solid-State Lett.*, **2(8)**, pp.390 (1999).
- [90] Zeng, Y., Russell, S. W., McKerrow, A. J., Chen, P., Alford, T. L., *Thin Solid Films*, **360(1-2)**, pp.283-292 (2000).
- [91] Zeng, Y., Russell, S. W., McKerrow, A. J., Chen, L., Alford, T. L., *J. Vac. Sci. Technol., B: Microelectron. Nanometer Struct. Process., Meas., Phenom.*, **18(1)**, pp.221-230 (2000).
- [92] Chang, T. C., Mor, Y. S., Liu, P. T., Tsai, T. M., Chen, C. W., Mei, Y. J., Sze, S. M., *Thin Solid Films*, **398**, pp.523-526 (2001).
- [93] Lee, H. J., Lin, E. K., Wang, H., Wu, W. L., Chen, W., Moyer, E. S., *Chem. Mater.*, **14(4)**, pp.1845-1852 (2002).
- [94] Penaud, J., Fruleux, F., Dubois, E., *Appl. Surf. Sci.*, **253(1)**, pp.395-399 (2006).
- [95] Chang, T. S., Chang, T. C., Liu, P. T., Chang, T. S., Yeh, F. S., *Thin Solid Films*, **498(1-2)**, pp.70-74 (2006).
- [96] Chang, T. S., Chang, T. C., Liu, P. T., Tsao, S. W., Yeh, F. S., *Thin Solid Films*, **516(2-4)**, pp.374-377 (2007).
- [97] Cord, B., Yang, J., Duan, H., Joy, D. C., Klingfus, J., Berggren, K. K. *J. Vac. Sci. Technol., B: Microelectron. Nanometer Struct. Process., Meas., Phenom.*, **27(6)**, pp.2616-2621 (2009).
- [98] Henschel, W., Georgiev, Y. M., Kurz, H., *J. Vac. Sci. Technol., B: Microelectron. Nanometer Struct. Process., Meas., Phenom.*, **21(5)**, pp.2018-2025 (2003).
- [99] Chen, Y., Yang, H., Cui, Z., *Microelectron. Eng.*, **83(4-9)**, pp.1119-1123 (2006).
- [100] Grigorescu, A. E., van der Krogt, M. C., Hagen, C. W., Kruit, P., *J. Vac. Sci. Technol., B: Microelectron. Nanometer Struct. Process., Meas., Phenom.*, **25(6)**, pp.1998-2003 (2007).
- [101] Yang, J. K., Berggren, K. K., *J. Vac. Sci. Technol., B: Microelectron. Nanometer Struct. Process., Meas., Phenom.*, **25(6)**, pp.2025-2029 (2007).
- [102] Sidorkin, V., van der Drift, E., Salemink, H., *J. Vac. Sci. Technol., B: Microelectron. Nanometer Struct. Process., Meas., Phenom.*, **26(6)**, pp.2049-2053 (2008).
- [103] Häffner, M., Haug, A., Heeren, A., Fleischer, M., Peisert, H., Chassé, T., Kern, D. P., *J. Vac. Sci. Technol., B: Microelectron. Nanometer Struct. Process., Meas.,*

- Phenom.*, **25(6)**, pp.2045-2048 (2007).
- [104] Lee, H. S., Wi, J. S., Nam, S. W., Kim, H. M., Kim, K. B., *J. Vac. Sci. Technol., B: Microelectron. Nanometer Struct. Process., Meas., Phenom.*, **27(1)**, pp.188-192 (2009).
- [105] Choi, S., Jin, N., Kumar, V., Adesida, I., Shannon, M., *J. Vac. Sci. Technol., B: Microelectron. Nanometer Struct. Process., Meas., Phenom.*, **25(6)**, pp.2085-2088 (2007).
- [106] Wi, J. S., Lee, T. Y., Jin, K. B., Hong, D. H., Shin, K. H., Kim, K. B., *J. Vac. Sci. Technol., B: Microelectron. Nanometer Struct. Process., Meas., Phenom.*, **24(6)**, pp.2616-2620 (2006).
- [107] Nam, S. W., Lee, T. Y., Wi, J. S., Lee, D., Lee, H. S., Jin, K. B., Kim, K. B., *J. Electrochem. Soc.*, **154(9)**, pp.H844 (2007).
- [108] Gnan, M., Thoms, S., Macintyre, D. S., De La Rue, R. M., Sorel, M., *Electron. Lett.*, **44(2)**, pp.115-116 (2008).
- [109] Guillorn, M., Chang, J., Fuller, N., Patel, J., Darnon, M., Pyzyna, A., Haensch, W., *J. Vac. Sci. Technol., B: Microelectron. Nanometer Struct. Process., Meas., Phenom.*, **27(6)**, pp.2588-2592 (2009).
- [110] Winston, D., Cord, B. M., Ming, B., Bell, D. C., DiNatale, W. F., Stern, L. A., Berggren, K. K., *J. Vac. Sci. Technol., B: Microelectron. Nanometer Struct. Process., Meas., Phenom.*, **27(6)**, pp.2702-2706 (2009).
- [111] Hobbs, R. G., Farrell, R. A., Bolger, C. T., Kelly, R. A., Morris, M. A., Petkov, N., Holmes, J. D., *ACS Appl. Mater. Interfaces*, **4(9)**, pp.4637-4642 (2012).
- [112] Memišević, E., Lind, E., Wernersson, L. E., *J. Vac. Sci. Technol., B: Microelectron. Nanometer Struct. Process., Meas., Phenom.*, **32(5)**, pp.051211 (2014).
- [113] Xiang, Q., Chen, Y., Wang, Y., Zheng, M., Li, Z., Peng, W., Duan, H., *Nanotechnology*, **27(25)**, pp.254002 (2016).
- [114] Gangnaik, A. S., Georgiev, Y. M., Collins, G., Holmes, J. D., *J. Vac. Sci. Technol., B: Microelectron. Nanometer Struct. Process., Meas., Phenom.*, **34(4)**, pp.041603 (2016).
- [115] Abuwasib, M., Lee, J. W., Lee, H., Eom, C. B., Gruverman, A., Singiseti, U., *J. Vac. Sci. Technol., B: Microelectron. Nanometer Struct. Process., Meas., Phenom.*, **35(2)**, pp.021803 (2017).
- [116] Solard, J., Chakaroun, M., Boudrioua, A., *J. Vac. Sci. Technol.*, **38(2)**, pp.022802 (2020).
- [117] Choi, S., Yan, M., Adesida, I., *Appl. Phys. Lett.*, **93(16)**, pp.163113 (2008).
- [118] Negrete, O. D., Onses, M. S., Nealey, P. F., Cerrina, F., *J. Vac. Sci. Technol., B: Microelectron. Nanometer Struct. Process., Meas., Phenom.*, **27(6)**, pp.3082-3087 (2009).
- [119] Fan, D., Ekinici, Y., *Proc. Extreme Ultraviolet (EUV) Lithography IV*, **9776**, pp.541-551 (2016).
- [120] Winter, A., Ekinici, Y., Götzhäuser, A., Turchanin, A., *2D Mater.*, **6(2)**, pp.021002 (2019).
- [121] Karim, W., Tschupp, S. A., Oezaslan, M., Schmidt, T. J., Gobrecht, J., van Bokhoven, J. A., Ekinici, Y., *Nanoscale*, **7(16)**, pp.7386-7393 (2015).
- [122] Ekinici, Y., Solak, H. H., David, C., Löffler, J. F., *Proc. Optomechatronic Micro/Nano Devices and Components III*, **6717**, pp.219-226 (2007).
- [123] Huang, J., Fan, D., Ekinici, Y., Padeste, C., *Microelectron. Eng.*, **141**, pp.32-36 (2015).
- [124] Kang, Y., Fukuoka, T., Takahashi, R., Utsumi, Y., Haruyama, Y., Matsui, S., *Microsyst. Technol.*, **20**, pp.1993-2000 (2014).
- [125] Louis, D., Nier, M. E., Fery, C., Heitzmann, M., Papon, A. M., Renard, S., *Microelectron. Eng.*, **61**, pp.859-865 (2002).
- [126] Lister, K. A., Thoms, S., Macintyre, D. S., Wilkinson, C. D. W., Weaver, J. M. R., Casey, B. G., *J. Vac. Sci. Technol., B: Microelectron. Nanometer Struct. Process., Meas., Phenom.*, **22(6)**, pp.3257-3259 (2004).
- [127] Stade, F., Heeren, A., Fleischer, M., Kern, D. P., *Microelectron. Eng.*, **84(5-8)**, pp.1589-1592 (2007).
- [128] Hessel, C. M., Summers, M. A., Meldrum, A., Malac, M., Veinot, J. G. C., *Adv. Mater.*, **19(21)**, pp.3513-3516 (2007).
- [129] Rodríguez Núñez, J. R., Kelly, J. A., Henderson, E. J., Veinot, J. G. C., *Chem. Mater.*, **24(2)**, pp.346-352 (2012).
- [130] Buriak, J. M., *Chem. Rev.*, **102(5)**, pp.1271-1308 (2002).
- [131] Yang, Z., Iqbal, M., Dobbie, A. R., Veinot, J. G. C., *J. Am. Chem. Soc.*, **135(46)**, pp.17595-17601 (2013).
- [132] Kelly, J. A., Veinot, J. G. C., *ACS Nano*, **4(8)**, pp.4645-4656 (2010).
- [133] Lundgren, S., Lutsenko, S., Jönsson, C., Moberg, C., *Org. Lett.*, **5(20)**, pp.3663-3665 (2003).
- [134] Dasog, M., De los Reyes, G. B., Titova, L. V., Hegmann, F. A., Veinot, J. G. C., *ACS Nano*, **8(9)**, pp.9636-9648 (2014).
- [135] Purkait, T. K., Iqbal, M., Wahl, M. H., Gottschling, K., Gonzalez, C. M., Islam, M. A., Veinot, J. G. C., *J. Am. Chem. Soc.*, **136(52)**, pp.17914-17917 (2014).
- [136] Beri, D., Busko, D., Mazilkin, A., Howard, I. A., Richards, B. S., Turshatov, A., *RSC Adv.*, **8(18)**, pp.9979-9984 (2018).
- [137] Heintz, A. S., Fink, M. J., Mitchell, B. S., *Adv. Mater.*, **19(22)**, pp.3984-3988 (2007).
- [138] Yu, Y., Fan, G., Fermi, A., Mazzaro, R., Morandi, V., Ceroni, P., Korgel, B. A., *J. Phys. Chem. C*, **121(41)**, pp.23240-23248 (2017).
- [139] Sychugov, I., Fucikova, A., Pevero, F., Yang, Z., Veinot, J. G. C., Linnros, J., *ACS Photonics.*, **1(10)**, pp.998-1005

- (2014).
- [140] Ono, T., Xu, Y., Sakata, T., Saitow, K. I. *ACS Appl. Mater. Interfaces*, **14**, pp.1373-1388 (2022).
- [141] Terada, S., Xin, Y., Saitow, K. I., *Chem. Mater.*, **32(19)**, pp.8382-8392 (2020).
- [142] Morozova, S., Alikina, M., Vinogradov, A., Pagliaro, M., *Front. Chem.*, **8**, pp.191 (2020).
- [143] Watanabe, J., Yamada, H., Sun, H. T., Moronaga, T., Ishii, Y., Shirahata, N., *ACS Appl. Nano Mater.*, **4(11)**, pp.11651-11660 (2021).
- [144] Cheong, I. T., Mock, J., Kallergi, M., Groß, E., Meldrum, A., Rieger, B., Becherer, M., Veinot, J. G. C., *Adv. Opt. Mater.*, **11(1)**, pp.2201834 (2023).
- [145] Friero, J. L., López-Vidrier, J., Blázquez, O., Ibáñez, J., Yazıcıoğlu, D., Gutsch, S., Hernández, S., *Sol. Energy Mater. Sol. Cells*, **230**, pp.111252 (2021).
- [146] Otsuka, M., Kurokawa, Y., Ding, Y., Juangsa, F. B., Shibata, S., Kato, T., Nozaki, T., *RSC Adv.*, **10(21)**, pp.12611-12618 (2020).
- [147] Ni, Z., Zhou, S., Zhao, S., Peng, W., Yang, D., Pi, X., *Mater. Sci. Eng. R: Rep.*, **138**, pp.85-117 (2019).
- [148] Romano, F., Angeloni, S., Morselli, G., Mazzaro, R., Morandi, V., Shell, J. R., Ceroni, P., *Nanoscale*, **12(14)**, pp.7921-7926 (2020).
- [149] Furey, B. J., Stacy, B. J., Shah, T., Barba-Barba, R. M., Carriles, R., Bernal, A., Downer, M. C., *ACS Nano*, **16(4)**, pp.6023-6033 (2022).
- [150] Alagarasan, J. K., Shasikala, S., Ganesan, S., Arunachalam, M., Manojkumar, U., Palaninaicker, S., Lo, H. M., *Environ. Res.*, **224**, pp.115402 (2023).